Reflection-Based Optical Fiber Strain Sensor Using Polarization Maintaining and Thin Core Fibers

D. Jauregui-Vazquez, J. P. Korterik, H. L. Offerhaus, J. M. Sierra-Hernandez, and J. A. Alvarez-Chavez

***Abstract*— A strain fiber optic sensor is proposed and experimentally demonstrated in this letter. The sensor operates in reflection mode, and its assembly relies on a single splice point between a thin core fiber and polarization-maintaining fiber. The system offers competitive sensitivities of 14.68 and 6.9 pm/$\mu\varepsilon$, determined by the PM-fiber length. In addition, the one-way ANOVA analysis indicates a minimal error (MSE=0.34) and low probability of measurement overlap (Prob > F = 5.59882 × 10^{-85}). The fabrication, the sensor dimensions, and the statistical analysis make the proposed sensor an attractive alternative for monitoring strain.**

***Index Terms*— Strain fiber optic sensor, polarization maintaining fiber, interferometric all fiber-optic device.**

I. Introduction

STRAIN receives special attention from the fiber-optic sensor community due to exciting applications such as biomechanical monitoring [1], medical surgery [2], structural health monitoring [3], robotics [4], metal deforming [5], and art preservation [6]. Diverse strain fiber optic sensors have been demonstrated over almost four decades. One of the first approaches to detect strain was the well-known Fiber Bragg Grating (FBG). These devices generally have a one integer digit sensitivity in terms of pm/$\mu\varepsilon$ [7]; Over the last decade, many efforts have focused on improving this sensitivity by modifying the FBG shape or combining it with interferometric devices [8]. Tapered optical fibers are another option to detect strain [9]. This thin fiber shows an improved sensitivity but needs delicate opto-mechanical handling.

Interferometric all-fiber devices emerge as a strain detection alternative with high sensitivity. Fabricating these devices is achieved by an arc splice technique using optical fibers with distinctive characteristics. Indeed, some of them have been presented as Mach-Zehnder, Sagnac, Fabry-Perot, and Michelson configurations. Some Mach-Zehnder and Michelson configurations show high sensitivity [10], [11]; Their fabrication often involves non-commercial optical fibers.

Fiber-optic Fabry-Perot interferometers based on air intracavity exhibit competitive sensitivities and low-temperature influence [12]. Sagnac interferometers offer a relatively simple implementation and can produce ultra-high sensitivity by extending the length of the sensing section [13], which limits some applications. The present manuscript proposes a reflection-based interferometric optical fiber structure for strain monitoring. The optical fiber structure is based on a single splice point between a thin core fiber and a polarization-maintaining fiber; they both are commercial products. The structure is reproducible and robust, and its fabrication is straightforward. Additionally, the sensitivity is competitive compared to other strain optical fiber sensors, and the statistical analysis indicates that minimal errors can be expected.

II. Sensing Setup and Principle of Operation

The proposed reflection-based optical fiber strain sensing setup is depicted in Figure 1. The interrogation system relies on the interconnection between three elements: an optical spectrometer (Advantest, AvaSpec-3648), a 50/50 optical fiber coupler (Thorlabs, TW1064R5F1B), and a broadband light source (Superlum, SLD-521-HP-PM; 930-160 nm, 5.8 mW). According to the fabricant, an output polarization state is excited by slow axis alignment (45° orientation).

The reflection-based strain fiber optic sensor is set at the end of the interrogation setup. This interferometric reflection optical fiber structure is achieved by splicing a thin core fiber (980HP) and a polarization-maintaining fiber (PM980-XP). The 980HP fiber has a core diameter of 3.6 μm and mode field diameter of 4.2 μm at 980 nm, whereas the PM980-XP has a core diameter of 5.5 μm and mode field diameter of 6.6 μm at 980 nm. Both fibers are designed for single-mode operation at 980nm and have a similar second mode cut-off around 920 nm. These fibers are spliced by using the multimode program of the Fitel S174H arc splicer (see inset in Figure 1).

The splice generates a mismatch point, where the core mode from the 980HP fiber splits into two orthogonally polarized modes, within the PM980-XP. These modes disperse throughout the polarization maintaining fiber and are reflected at the flat end-face via Fresnel reflection. Upon their return, these modes are coupled back into the 980HP core at the splicing

Manuscript received 15 August 2022; accepted 8 September 2022. Date of publication 14 September 2022; date of current version 27 September 2022. The work of D. Jauregui-Vazquez was supported in part by the Consejo Nacional de Ciencia y Tecnologia (CONACYT) through the Sabbatical Support under Grant 290595. *(Corresponding author: J. A. Alvarez-Chavez.)*

D. Jauregui-Vazquez is with the Optical Sciences Group, University of Twente, 7522 NB Enschede, The Netherlands, and also with the División de Ingenierías Campus Irapuato Salamanca, Departamento de Ingeniería Electrónica, Universidad de Guanajuato, Salamanca, Guanajuato 36885, Mexico (e-mail: d.jaureguivazquez@utwente.nl).

J. P. Korterik, H. L. Offerhaus, and J. A. Alvarez-Chavez are with the Optical Sciences Group, University of Twente, 7522 NB Enschede, The Netherlands (e-mail: j.p.korterik@utwente.nl; h.l.offerhaus@utwente.nl; j.a.alvarezchavez@utwente.nl).

J. M. Sierra-Hernandez is with the División de Ingenierías Campus Irapuato Salamanca, Departamento de Ingeniería Electrónica, Universidad de Guanajuato, Salamanca, Guanajuato 36885, Mexico (e-mail: jm.sierrahernandez@ugto.mx).

Color versions of one or more figures in this letter are available at https://doi.org/10.1109/LPT.2022.3206011.

Digital Object Identifier 10.1109/LPT.2022.3206011

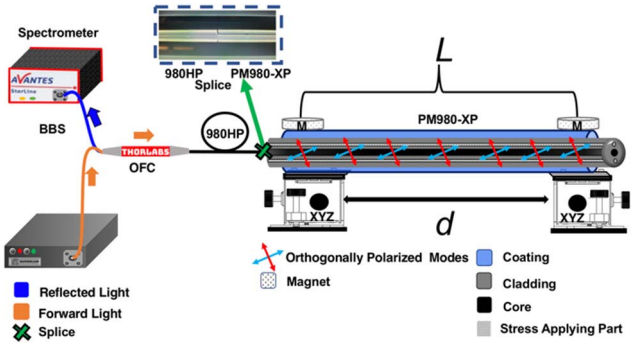

Fig. 1. Schematic configuration of the reflection-based strain fiber optic sensor based on interferometric device. Inset: Splice between the thin core fiber and the polarization maintaining fiber.

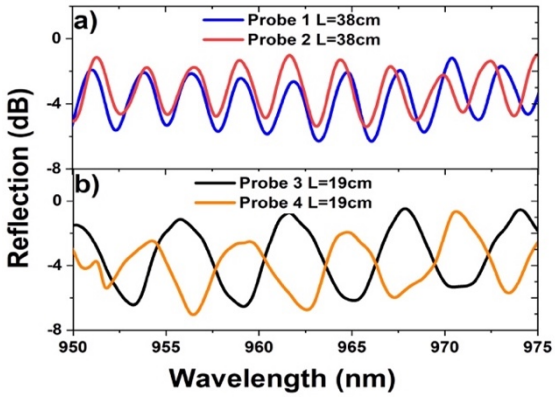

Fig. 2. Reflection based interference spectra of interferometers with a PM980-XP length of (a)38 cm and (b)19 cm.

point. It is essential to mention that initial polarization from the broad band source stage is crucial to excite the interference. Their interaction generates an interference reflection spectrum that can be determined by:

$$I_R = I_a + I_b + 2(I_a I_b)^{0.5}\cos(\varphi). \tag{1}$$

where I_a and I_b are the orthogonally polarized modes generated at the splice point; the phase ($\varphi = 4\pi BL/\lambda$) between these modes will depend on the length (L) and the birefringence coefficient (B) of the PM980-XP, as well as on the operation wavelength (λ). The minima in the reflection interference spectrum are governed by:

$$\lambda_d = \frac{4BL}{2k+1}. \tag{2}$$

where k represents an integer value. When the birefringence is altered, the minima will be shifted. Furthermore, by considering two minima points, it is possible to obtain the Free-Spectral Range (FSR, $\Delta\lambda$) as:

$$FSR = \frac{\lambda_{d1} * \lambda_{d2}}{2BL}. \tag{3}$$

III. Results

Four samples were fabricated for validation: Two with a PM980-XP length of 38 cm and two more with a length of 19 cm. Their interference reflection spectra are shown in Figure 2. The samples with a 38 cm length showed a similar FSR of around 3 nm (Figure 2a); meanwhile, the samples with a length of 19 cm had an FSR of 6 nm (Figure 2b). These values agree with the FSR relation in that as the length of the PM980-XP decreases, the FSR increases. Moreover, if we consider the beat length, it is possible to obtain information about the birefringence. According to the manufacturer, the beat length of the PM980-XP is $\leq$2.7 mm at 980 nm. Then, the B value will be close to 3.63×10^{-4}. The FSR of the four samples yields similar B values, close to 4.21×10^{-4}. Due to the slight birefringence difference (5×10^{-5}) between the theoretical and the experimental values, it can be assumed that the two orthogonally polarized modes generate the interference reflection spectrum. The visibility of the fabricated samples oscillates between 5 and 3 dB. It is important to mention that the phase difference observed in Figure 2b can be attributed to the axis orientation of the PM980-XP. All the samples were tested for strain; here, two XYZ translation stages were used to hold the reflection-based interferometric devices. Then, the distance between both translation stages (D) is increased or decreased. As a result, the strain is controlled. It worth mentioning that the coating of the PM980-XP was not removed during the experiments. In addition, we employ magnets to hold the PM980-XP at the v-grove fiber holder; these magnets are located over the coated region (see Fig. 1).

The strain response of probe 2 (with a length of 38 cm) is shown in Figure 3a. As the strain increases, the interference reflection spectrum is shifted to longer wavelengths. This sample exhibits a total wavelength shifting of 6.91 nm at the strain range from 0 to 370 $\mu\varepsilon$. The wavelength shift has to do with birefringence change due to the elasto-optic effect. Moreover, the shifting direction is linked to the increment of the birefringence. Probe 3 was also analyzed under a maximum strain of 1428 $\mu\varepsilon$ (Figure 3b); this sample provides a total wavelength shift of 9.17 nm. This sample has a length of 19 cm. Both samples present the same wavelength shift direction; however, their sensitivities will be different due to their dimensions. The strain was applied in the forward and backward direction three times for samples 1 and 2; then, the sensitivities were analyzed considering the wavelength shift of the minima close to 957 nm (Probe1 and Probe2). The maximum sensitivity in the forward direction analysis for Probe1 was 14.68 pm/$\mu\varepsilon$ with an adjusted R-square (R^2) of 0.9957 (see Figure 4a). At the same time, the backward analysis of Probe 1 indicates a minimum sensitivity of 14.37 pm/$\mu\varepsilon$ with $R^2 = 0.9852$. As a result, the hysteresis is 0.26 nm. Probe 2 shows maximum sensitivity of 14.28 pm/$\mu\varepsilon$ in the forward direction and 14.06 pm/$\mu\varepsilon$ in the backward direction (see Figure 4b). The forward and backward analyses of Probe 2 indicate an adjusted R-square of 0.9694 and 0.9839, respectively. This sample exhibit a hysteresis of 0.7 nm. The same analysis was conducted on sample 3 (Figure 5a) and 4 (Figure 5b). In these experiments, we consider minima points at: 952 nm-Probe3 and 956 nm-Probe4. Here, sample 3 shows a maximal sensitivity of 6.9 pm/$\mu\varepsilon$ ($R^2 = 0.9904$) in the forward direction, and 6.7 pm/$\mu\varepsilon$ ($R^2 = 0.9920$) in the backward direction. Then, minimal hysteresis of 0.5 nm is observed. Sample 4 shows a maximal hysteresis of 1nm; resulting in lower adjusted R-square values of 0.9767 and 0.9845 in the

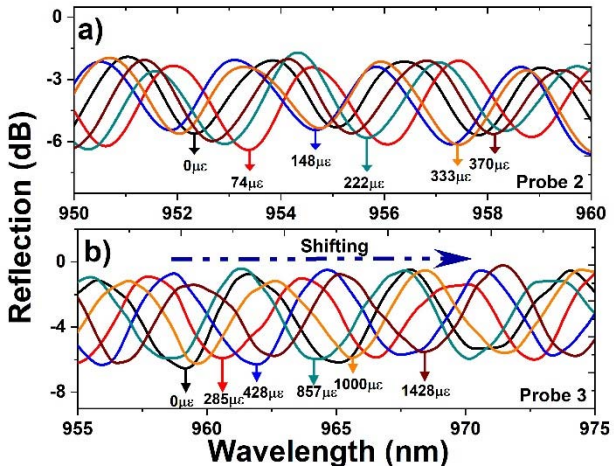

Fig. 3. Interference reflection spectrum response as the strain is applied using a) probe2 and b) probe3.

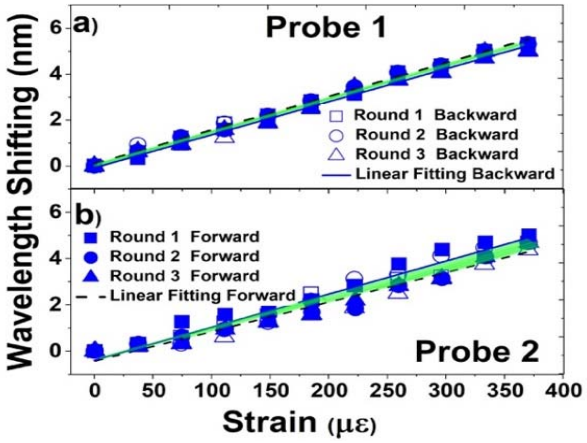

Fig. 4. Repeatability strain experiments and their hysteresis variation of a) probe1 and b) probe2.

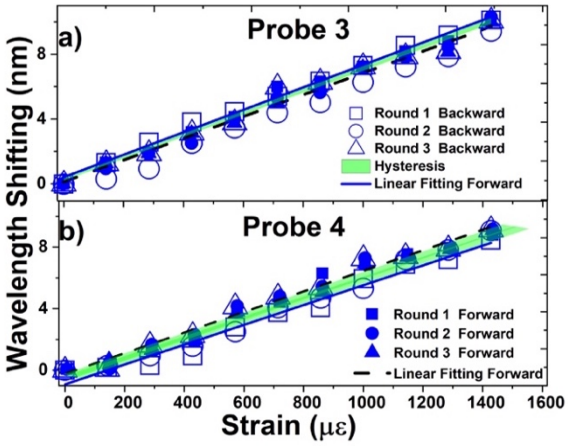

Fig. 5. Wavelength shifting response after three rounds forward-backward direction of a) probe 3 and b) probe 4.

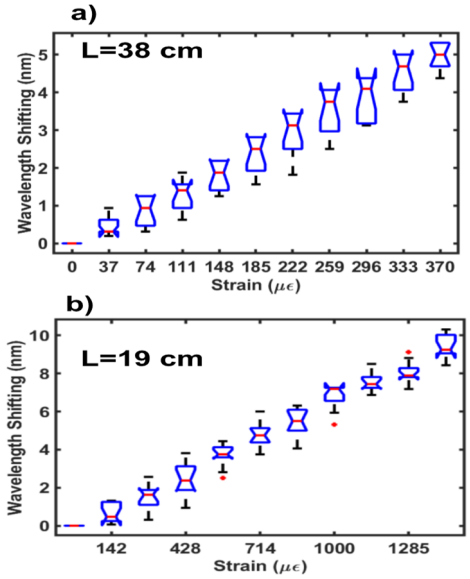

Fig. 6. Anova analyses for strain sensor with a length of a) 38 cm and b) 19 cm.

forward and backward directions, respectively. Nevertheless, the sensitivity remains almost similar at 6.7 pm/$\mu\varepsilon$, in both directions.

Considering that the samples show similar sensitivities according to the length of the PM980-XP, the data can be analyzed using the one-way ANOVA method in MATLAB. The ANOVA results of Probe1 and Probe 2 are depicted in Figure 6a. It can be observed that the means have a lower probability of overlapping (Prob $>$ F $= 1.22634 \times 10^{-67}$). Furthermore, the error presented can be attributed to the initial strain setting at the moment to fix the samples (-Mean Square Error-MSE=0.1901). According to Figure 6b, samples 3 and 4 show an MSE=0.34, which can be attributed to the unexpected data measured at high strain values (see Figure b); these samples show lower Prob $>$ F $= 5.59882 \times 10^{-85}$. Please note that the above results were achieved at room temperature. Please note that the coating of the PM980-XP can be affected by the tensile strength after several rounds, then the sensor performance can be compromised. As a result, it is necessary to monitor the sensitivity for a longer time; then, a new sample with high sensitivity was fabricated (14 pm/$\mu\varepsilon$). Subsequently, the strain was monitored, and the following experiment was performed once per week for three weeks: the strain was applied two times in the forward direction and one time in a backward direction; the sensitivity variation during these analyses can be appreciated in Figure 7.

As it can be appreciated, the sensitivity is not severely affected. Moreover, the hysteresis variation remains similar (0.7nm). However, the results indicate an initial point variation. As a result, the fiber optic sensor requires a calibration process. These undesired effects can be attributed to the translation stage's hysteresis and the coating affectation. One alternative to overcome these effects can be the phase signal analysis [14]; here, it has been demonstrated that the phase analysis reduces the use of an initial set point. Furthermore, other computational techniques can be explored to avoid calibration [15]. Moreover, the package requires special characteristics that would optimize the sensor performance [16].

IV. Discussion

Several interferometric optical fiber structures have been proposed using polarization-maintaining fibers; as a result, good sensor performance can be achieved [11], [17], [18]. Nevertheless, the polarization optical fiber design and fabrication accessibility, limit the viability and the capacity for

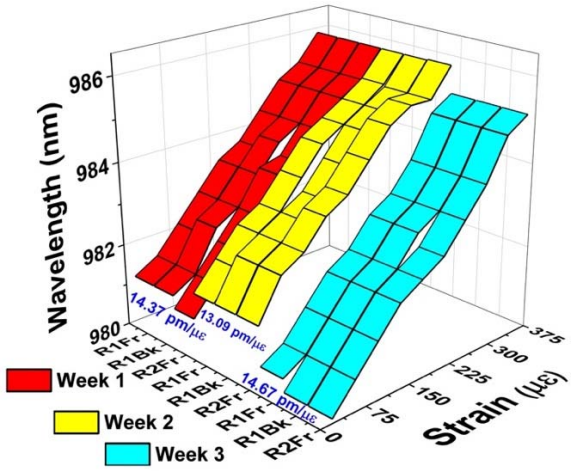

Fig. 7. Long time strain sensitivity analysis.

TABLE I
COMPARTIVE PERFORMACE WITH RECENT WORKS

Ref.	Sensitivity (pm/με)	Range (με)	Year
[10]	10.65	200-550	2019
[20]	5.4	0-6800	2022
[21]	1.57	0-800	2022
[22]	11.5	0-5385	2022
[23]	6.63	0-800	2021
[24]	15.06	0-4508	2022
This Work	14.68	0-370	2022

studying these devices. In recent years, sensitivities with three integer digits were demonstrated via the Vernier effect [13], so almost any interferometric fiber optic sensor sensitivity could be improved. The maximal sensitivity achieved in this work is 14.68 pm/$\mu\varepsilon$ ($R^2 = 0.9957$). As shown in Table I, this sensitivity is competitive with recent works. In addition, this sensitivity can be magnified by an artificial reference spectrum using Fast Fourier Transform [19].

REFERENCES

[1] P. Roriz, L. Carvalho, O. Frazão, J. L. Santos, and J. A. Simões, "From conventional sensors to fibre optic sensors for strain and force measurements in biomechanics applications: A review," *J. Biomech.*, vol. 47, no. 6, pp. 1251–1261, 2014.

[2] A. Handelman, Y. Keshet, E. Livny, R. Barkan, Y. Nahum, and R. Tepper, "Evaluation of suturing performance in general surgery and ocular microsurgery by combining computer vision-based software and distributed fiber optic strain sensors: A proof-of-concept," *Int. J. Comput. Assist. Radiol. Surg.*, vol. 15, no. 8, pp. 1359–1367, Aug. 2020.

[3] R. B. Figueira, J. M. de Almeida, B. Ferreira, L. Coelho, and C. J. R. Silva, "Optical fiber sensors based on sol–gel materials: Design, fabrication and application in concrete structures," *Mater. Adv.*, vol. 2, no. 22, pp. 7237–7276, 2021.

[4] H. Bai, S. Li, J. Barreiros, Y. Tu, C. R. Pollock, and R. F. Shepherd, "Stretchable distributed fiber-optic sensors," *Science*, vol. 370, no. 6518, pp. 848–852, Nov. 2020.

[5] B. Bednarz, P. Popielski, R. Sieńko, T. Howiacki, and Ł. Bednarski, "Distributed fibre optic sensing (DFOS) for deformation assessment of composite collectors and pipelines," *Sensors*, vol. 21, no. 17, p. 5904, Sep. 2021.

[6] W. Zawadzki, M. Bartosik, K. Dzierżga, Ł. Bratasz, M. Łukomski, and E. Peacock, "Application of fiber Bragg gratings for strain measurement in historic textiles and paintings on canvas," *Opt. Appl.*, vol. 42, no. 3, pp. 503–517, 2012.

[7] R. Li, Y. Chen, Y. Tan, Z. Zhou, T. Li, and J. Mao, "Sensitivity enhancement of FBG-based strain sensor," *Sensors*, vol. 18, no. 5, pp. 1–12, 2018.

[8] X. Zhao *et al.*, "Ultra-high sensitivity and temperature-compensated Fabry–Perot strain sensor based on tapered FBG," *Opt. Laser Technol.*, vol. 124, Apr. 2020, Art. no. 105997.

[9] J. R. Ek-Ek *et al.*, "Dual tapered optical fiber for simultaneous detection of curvature and strain," *Opt. Fiber Technol.*, vol. 69, Mar. 2022, Art. no. 102843.

[10] Z. Tang, S. Lou, X. Wang, W. Zhang, S. Yan, and Z. Xing, "High-performance bending vector and strain sensor using a dual-tapered photonic crystal fiber Mach–Zehnder interferometer," *IEEE Sensors J.*, vol. 19, no. 11, pp. 4062–4068, Jun. 2019.

[11] X. Tan, Y. Geng, and X. Li, "High-birefringence photonic crystal fiber Michelson interferometer with cascaded fiber Bragg grating for pressure and temperature discrimination," *Opt. Eng.*, vol. 55, no. 9, Sep. 2016, Art. no. 090508.

[12] L. Cai, J. Wang, M. Chen, and X. Ai, "A high-sensitivity strain sensor based on an unsymmetrical air-microbubble Fabry–Pérot interferometer with an ultrathin wall," *Measurement*, vol. 181, Aug. 2021, Art. no. 109651.

[13] W. Zhang *et al.*, "Highly sensitive temperature and strain sensor based on fiber Sagnac interferometer with Vernier effect," *Opt. Commun.*, vol. 506, Mar. 2022, Art. no. 127543.

[14] M. Gutierrez-Rivera *et al.*, "Low-pressure fiber-optic sensor by polyester Fabry–Perot cavity and its phase signal processing analysis," *Sens. Actuators A, Phys.*, vol. 315, Nov. 2020, Art. no. 112338.

[15] S. Urban, M. Ludersdorfer, and P. van der Smagt, "Sensor calibration and hysteresis compensation with heteroscedastic Gaussian processes," *IEEE Sensors J.*, vol. 15, no. 11, pp. 6498–6506, Nov. 2015.

[16] P. Zhu, X. Xie, X. Sun, and M. A. Soto, "Distributed modular temperature-strain sensor based on optical fiber embedded in laminated composites," *Compos. B, Eng.*, vol. 168, pp. 267–273, Jul. 2019.

[17] M. Zhu, H. Murayama, D. Wada, and K. Kageyama, "Dependence of measurement accuracy on the birefringence of PANDA fiber Bragg gratings in distributed simultaneous strain and temperature sensing," *Opt. Exp.*, vol. 25, no. 4, p. 4000, 2017.

[18] X. He, C. Ma, X. Wang, Z. Wang, and L. Yuan, "Pressure vector sensor based on an orthogonal optical path Sagnac interferometer," *Opt. Exp.*, vol. 28, no. 6, p. 7969, 2020.

[19] X. Fang *et al.*, "Signal processing assisted Vernier effect in a single interferometer for sensitivity magnification," *Opt. Exp.*, vol. 29, no. 8, p. 11570, 2021.

[20] C. Lu *et al.*, "A compact fiber-based sensor for wide range strain measurement," *Opt. Laser Technol.*, vol. 148, pp. 1–8, Aug. 2022.

[21] F. Lan and D. N. Wang, "Long-period fiber grating based on inner microholes in optical fiber," *Opt. Lett.*, vol. 47, no. 1, p. 146, 2022.

[22] J. Wang *et al.*, "High-sensitivity micro-strain sensing using a broadband wavelength-tunable thulium-doped all-fiber structured mode-locked laser," *Opt. Lett.*, vol. 47, no. 1, p. 34, 2022.

[23] S.-C. Yan, Y. Zhao, M.-Q. Chen, and Q. Liu, "Optical fiber strain sensor with double S-tapers," *Instrum. Sci. Technol.*, vol. 49, no. 3, pp. 313–326, May 2021.

[24] X. Chen *et al.*, "Sensitivity-enhanced strain sensor with a wide dynamic range based on a novel long-period fiber grating," *IEEE Sensors J.*, vol. 22, no. 4, pp. 3196–3201, Feb. 2022.